REPORT DOCUMENTATION PAGE

Form Approved
OMB No. 0704-0188

1. REPORT DATE *(DD-MM-YYYY)*	**2. REPORT TYPE**	**3. DATES COVERED** *(From - To)*
31-07-2013	Final Report	8/1/2010-7/31/2013

4. TITLE AND SUBTITLE

Prognosis of Long-Term Load-Bearing Capability in Aerospace Structures: Quantification of Microstructurally Short Crack Growth

5a. CONTRACT NUMBER
AFOSR FA9550-10-1-0213

5b. GRANT NUMBER
AFOSR FA9550-10-1-0213

5c. PROGRAM ELEMENT NUMBER

6. AUTHOR(S)

A. D. Rollett
Department of Materials Science and Engineering, Carnegie Mellon University, PA, USA

A. R. Ingraffea

5d. PROJECT NUMBER

5e. TASK NUMBER

5f. WORK UNIT NUMBER

7. PERFORMING ORGANIZATION NAME(S) AND ADDRESS(ES)

Carnegie Mellon Univ., 5000 Forbes Ave., Pittsburgh, PA ; Cornell University, Ithaca, NY

8. PERFORMING ORGANIZATION REPORT NUMBER

9. SPONSORING / MONITORING AGENCY NAME(S) AND ADDRESS(ES)

AFOSR

10. SPONSOR/MONITOR'S ACRONYM(S)

11. SPONSOR/MONITOR'S REPORT NUMBER(S)

12. DISTRIBUTION / AVAILABILITY STATEMENT

Public Release OK

13. SUPPLEMENTARY NOTES

14. ABSTRACT

Carnegie Mellon and Cornell Universities collaborated to investigate the behavior of microstructurally small cracks under cyclic loading with the aim of improving our understanding of the substantial fraction of fatigue life occupied by the crack initiation phase. Heavy use was made of advanced tools such as High Energy Diffraction Microscopy (HEDM) for 3D mapping of microstructures in the materials of interest, namely Ni-based superalloys such as LSHR and René88DT. We worked closely with partners at AFRL and GE Global Research to obtain suitable specimens for characterization and simulation. LSHR samples with multiple microcracks provided valuable information that established that fatigue cracks start on or close to coherent twin boundaries ("annealing twins") in large grains where the twin-parallel slip systems are well aligned with respect to the loading direction. This conformation was then tested via finite element simulation to determine which criterion could be most reliable for predicting the development of microcracks. By employing a constitutive relation that accounts for the effect of plastic deformation gradient, which arise from accommodating the evolution of slip close to twin boundaries. The results show that simulation can effectively reproduce the concentration of slip parallel to twin boundaries that is characteristic of crack initiation. Some work was also performed to determine the appropriate size of a simulation volume when a particular location in

15. SUBJECT TERMS

16. SECURITY CLASSIFICATION OF:			**17. LIMITATION OF ABSTRACT**	**18. NUMBER OF PAGES**	**19a. NAME OF RESPONSIBLE PERSON**
a. REPORT	**b. ABSTRACT**	**c. THIS PAGE**			**19b. TELEPHONE NUMBER** *(include area code)*

Prognosis of Long-Term Load-Bearing Capability in Aerospace Structures: Quantification of Microstructurally Short Crack Growth

AFOSR FA9550-10-1-0213

Final Report

Prepared By:

A. D. Rollett
Department of Materials Science and Engineering, Carnegie Mellon University, PA, USA

A. R. Ingraffea
School of Civil and Environmental Engineering, Cornell University, NY, USA

July 31, 2013

Abstract

Carnegie Mellon and Cornell Universities collaborated to investigate the behavior of *microstructurally small cracks* under cyclic loading with the aim of improving our understanding of the substantial fraction of fatigue life occupied by the crack initiation phase. Heavy use was made of advanced tools such as High Energy Diffraction Microscopy (HEDM) for 3D mapping of microstructures in the materials of interest, namely Ni-based superalloys such as LSHR and René88DT. We worked closely with partners at AFRL and GE Global Research to obtain suitable specimens for characterization and simulation. LSHR samples with multiple microcracks provided valuable information that established that fatigue cracks start on or close to coherent twin boundaries ("annealing twins") in large grains where the twin-parallel slip systems are well aligned with respect to the loading direction. This conformation was then tested via finite element simulation to determine which criterion could be most reliable for predicting the development of microcracks. By employing a constitutive relation that accounts for the effect of plastic deformation gradient, which arise from accommodating the evolution of slip close to twin boundaries. The results show that simulation can effectively reproduce the concentration of slip parallel to twin boundaries that is characteristic of crack initiation. Some work was also performed to determine the appropriate size of a simulation volume when a particular location in a sample is known to be of interest. In the example of the HEDM image of LSHR, the size of the volume around the location of a microcrack was investigated with the result that for convergence of the elastic stress (and strain) fields, more than 250 grains around the microcrack needed to be included in the simulation volume.

1. Introduction

1.0 The Project

The focus of this DCT project was on quantifying the origins and growth rates of microstructurally short fatigue cracks. It aimed to provide quantification of the variability of fatigue lifetime in aircraft components, which is associated with the early stages of fatigue crack growth (Newman, 2000). Work started at the end of summer 2010 with bringing graduate students on board at both CMU and Cornell. We partnered with both AFRL (Reji John, Sushant Jha, and Ravi Chona) and with General Electric Research (principally Tim Hanlon, Jim Laflen and Adrian Loghin, with occasional interactions with Andrew Deal and Deb Whitis). The effort at CMU focused on characterization of a nickel-based superalloys, both LSHR (from AFRL) and Rene 88DT (from GE), as well as synthetic 3D microstructures for use in simulation. Cornell used information provided by CMU such as the synthetic microstructures, or parts of measured microstructures to perform simulations that aimed to replicate the observed behavior and thereby develop the micromechanics models needed for quantification of short fatigue crack behavior.

1.1 Prior Work by Other Researchers

A number of researchers have considered the question of the unexpected initiation of cracks along twin boundaries in fcc metals. Neumann and coworkers have developed a simplified model to calculate local stress concentrations near twin boundaries in stainless steel, based on elastic stress incompatibilities across the boundaries (Neumann and Tonnessen, 1987; Heinz and Neumann, 1990; Neumann, 1999). Their approach was limited in the ability to measure grain orientation for the number of grains which are readily characterized using current techniques; however, they report a high success rate in predicting whether or not a crack might develop. Their stress analysis was, however, purely analytical and did not take into account a full, realistic polycrystalline structure.

Laird and colleagues have also addressed the role of annealing twin boundaries in fcc materials, considering both compatibility stresses and also TEM studies of persistent slip bands (1992, 1997). This work follows up on the proposal by Thompson that local changes in the dislocation structure in the vicinity of twin boundaries could be responsible for their susceptibility to cracking, as opposed to the stress incompatibility models of Neumann, et al. These studies, it should be noted, have all focused on fcc materials subjected to high-cycle fatigue loading.

Aubin and coworkers have performed an analysis of microcrack initiation in austenitic stainless steel subjected to low-cycle fatigue (2008, 2009, 2010). Although initiation along twin boundaries accounts for only a small portion of initiation sites in these specimens, their studies include an analysis of Schmid factors similar to that presented later in this document. This analysis is however limited to crack-initiating grains, and not the larger distributions presented below.

More recent work by Pollock, Jones and coworkers has involved TEM studies of René88DT subjected to ultrasonic fatigue tests (2009, 2012). Their work points to the importance of $\Sigma 3$ grain boundaries in large grains with high Schmid factors, with nearly all cracks occurring at

such locations within the microstructure. More specifically, their work points to crack initiation occurring close to, but not at the grain boundaries, with evidence of precipitate shearing within approximately 100 nm of the actual boundaries, which they interpret as evidence of cyclic strain localization.

2. Characterization

2.1 Material and Fatigue Testing

Fatigue specimens were provided courtesy of the Air Force Research Laboratory of Wright-Patterson Air Force Base, Dayton, Ohio. The material for test specimens was provided to AFRL via NASA.

The specimens are 3 mm wide, flat dog bone samples of the advanced disk superalloy LSHR (low solvus, high refractory). The nominal composition of LSHR in weight percent is 3.5Al, 0.03 B, 0.03C, 20.7Co, 12.5Cr, 2.7Mo, 1.5Nb, 1.6Ta, 3.5Ti, 4.3W, 0.05Zr, balance Ni (Gabb *et al.*, 2005). The processing consisted of atomization in argon, with atomized powder being passed through screens of -270 mesh to give powder particle diameters of no more than about 55 μm. The powder is then sealed in a stainless steel container, hot compacted, and extruded at a reduction ratio of 6:1. Rods of 0.5-inch diameter and about 6-inch length were induction heated in the middle region above the gamma prime solvus temperature to produce a supersolvus, coarse grain structure. Thin (approximately 1 mm thickness) specimens were then EDM-machined from these rods. Average grain size in the coarse-grained and fine-grained regions were approximately 23 μm and 4 μm respectively. A backscatter electron image of the microstructure showing gamma prime, as well as an example of a surface microcrack, is depicted in Figure 2.1.

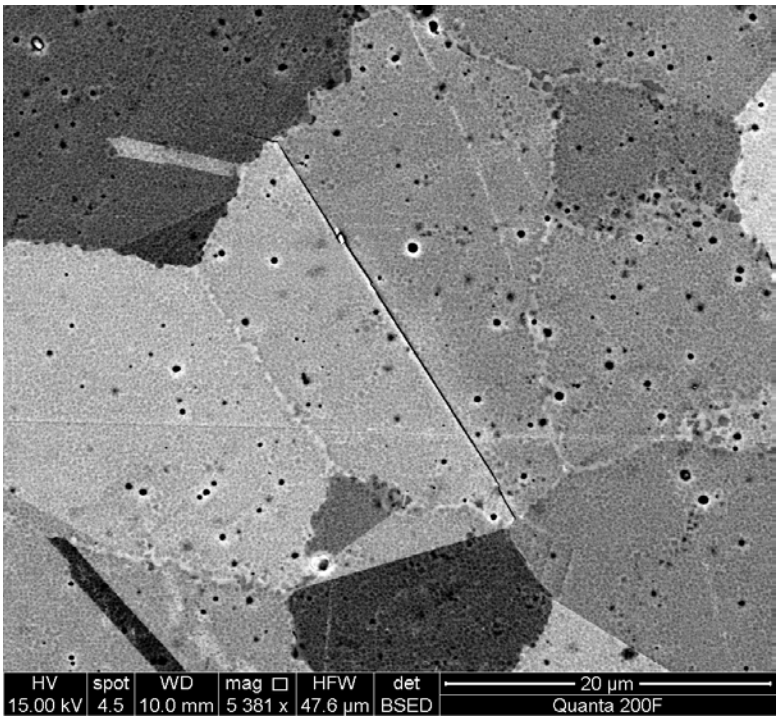

Figure 2.1. Backscatter electron image of a surface microcrack, also depicting gamma prime size and distribution.

The test specimens were fatigued in tension-tension under conditions sufficient to generate surface cracks (test parameters are given in Table 2.1). One of the test specimens was sectioned in support of efforts to characterize and analyze the three-dimensional microstructure.

Table 2.1 Fatigue test parameters

maximum stress	1050 MPa
stress ratio, R	0.05
frequency	10 Hz
temperature	23 ˚C
number of cycles, N	37,500

2.2 Characterization

2.2.1 Automated EBSD and High Energy Diffraction Microscopy

Automated electron backscatter diffraction (EBSD) and high energy diffraction microscopy (HEDM) were used to characterize the samples. EBSD is a now-standard technique performed in the SEM to probe the surface of a specimen and provide lattice orientation information, or Euler angles, on a regular, discrete grid. All of the 2d analysis was based on EBSD surface mapping. HEDM is a much newer technique which takes advantage of the very high-energy x-rays available from a synchrotron source, in this case the Advanced Photon Source (APS) at Argonne National Laboratory (Suter *et al.*, 2006 and 2008, Lienert *et al*., 2007). In HEDM, the sample, with approximate cross-sectional diameter of 1 mm, is probed by a focused high-energy x-ray beam. The typical collimated beam height is 4 μm, with a beam width sufficient to illuminate the entire cross-section as it moves through 180◦ of rotation about the vertical axis. The experiment involves the collection of a series of diffractograms by a near-field detector, first with a well-characterized calibration specimen, then with the sample. For each layer, 180 images are collected, each one as the sample sweeps through a one-degree rotation, for each of at least two detector distances.

The actual reconstruction of the three-dimensional orientation map relies on a forward modeling algorithm. The experimental setup is simulated by the reconstruction software, including the beam, sample and detector, using optical parameters determined from the calibration specimen data, and later refined by the algorithm. The process involves creating a sample grid, and simulating the diffraction due to any one voxel, for the entire crystallographic orientation space. The simulated diffraction is compared to the actual data and a best fit selected. This is a computationally intensive, but readily parallelized operation, and one for which the resulting indexed orientations are highly overdetermined. The end result is an orientation map with high angular resolution (approx. 0.1◦).

The large-area EBSD mapping of these surface cracks provided the orientation information necessary for both the boundary analysis, a description of which follows, and as input for the elastic FFT simulation. The spectral method is an alternative to finite element modeling, used in this instance because of its convenience and speed. The FFT-based elastic simulation code was

developed by R. Lebensohn (2001), based upon a simulation model developed by Moulinec and Suquet (1998) for the analysis of composite structures. This simulation approach was adopted in the present study due to a number of important features. First, most characterization techniques yield microstructural data on a discretized grid. The FFT-based approach takes an orientation map as direct input, precluding the need for a mesh generation procedure as with finite element-based simulations. In addition, improvements in characterization techniques, specifically in 3D characterization, have led to increasingly large datasets requiring more efficient simulation techniques. The FFT-based approach is much less computationally intensive, with results which have been shown to compare favorably to finite element simulations (Prakash and Lebensohn, 2009). The simulation of elastic stress response imposes a strain boundary condition, and the reported stress values will of course depend on the amount of strain. As it is a purely elastic calculation with no regard for the yield stress, the relative values of stress on different systems, as affected by the elastic anisotropy, are of importance rather than the absolute values.

2.2.2 Segmentation and smoothing

The boundary analysis consists of grain identification using the commercial TSL EBSD analysis software, followed by smoothing of boundary segments using in-house code which also segments boundaries by type according to their coincident site lattice (CSL) Σ designation. The Σ3 boundaries were further sorted into a list of likely coherent boundaries by calculation of the surface trace normal.

The code used for boundary smoothing and segmentation was developed by Lee, and the particular approach used here was adapted from that used in the analysis of heterophase interfaces, as described by Lee *et al* (2012). The smoothing of boundaries uses a two-dimensional version of a 3d marching cubes algorithm (Lorensen *et al.*, 1987). To summarize, the algorithm first identifies nodes and edges within the structure, then attempts to approximate the boundary shapes by smoothing the edges while maintaining local curvature between the nodes.

2.2.3 Σ3 and coherent Σ3 identification

The Σ3 designation is notation derived from the CSL model for the description of grain boundaries. The coincident site lattice model is one attempt at explaining the properties of various 'special' boundaries, in a variety of contexts. Here it is simply important to note that the model derives from the notion that grain boundary properties are influenced by the structure at grain boundaries, with a high degree of atomic coincidence across a boundary expected to correlate with properties such as low interfacial energy and resistance to cracking. Boundaries which have an axis-angle misorientation relationship of 60◦, about a common [111] rotation axis expressed in the crystal coordinates of the misoriented grains, are Σ3 boundaries.

Although identifying a Σ3 misorientation relationship is relatively straightforward using the Euler angles of an orientation map, the further segmentation by coherent Σ3 boundary requires the boundary surface trace obtained via the smoothing operation. Grain boundaries can be described not only in terms of misorientation (either a 1-parameter angle description, or a 3-parameter axis- angle relationship), but also by the characterization of the boundary plane as well. Although reliably characterizing the boundary plane requires a three-dimensional

orientation map such as the HEDM technique described above, we can identify likely coherent boundaries using only a 2d orientation mapping.

The orientation of the boundary plane distinguishes a coherent Σ3 from a Σ3. The coherent boundary can be visualized as a pure twist relationship between grains. The common [111] crystal axis, about which one lattice appears rotated by 60◦ relative to the other, must be perpendicular to the plane of the boundary. This is in contrast to a pure tilt boundary, for instance, for which the [111] direction of each crystal lies within the plane of the grain boundary. In that case the boundary plane might be inclined in a variety of different orientations, and combinations of pure twist and pure tilt are of course also possible. But the pure twist, coherent boundary is a clear, fixed relationship which results in excellent atomic coincidence and low GB energy.

The test for coherency can then be visualized by considering a surface trace vector, v, and the direction of the common [111] misorientation axis, n. Mathematically, the grains and surface trace must satisfy the condition $v \cdot n = 0$, or more specifically, $v \cdot n \leq \cos(90 - \theta)$, where θ is some angular threshold value. Although the boundary surface trace does not provide information about the inclination of the boundary beneath the surface, this criterion does at least allow us to identify candidate coherent boundaries, which have generally been referred to as coherent boundaries throughout this document.

2.3 Results and Analysis

The observed microcracks occur along likely coherent Σ3 boundaries, oriented favorably for slip as indicated by relatively high Schmid factor values. Such boundaries have surface traces inclined at nearly 45◦ relative to the tensile direction of the fatigue test. Figure 2.2 depicts one of the cracks, and the corresponding EBSD map appears in Figure 2.3, with the horizontal direction corresponding to the specimen tensile axis.

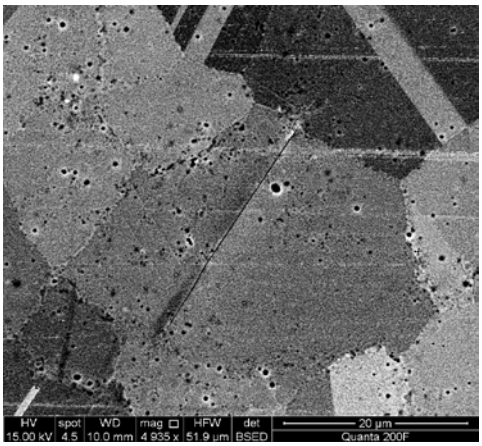

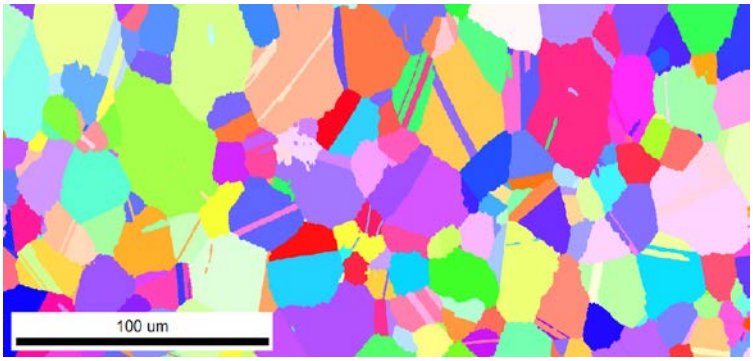

Figures 2.2 (left) and 2.3 (right). BSE image of a microstructurally small fatigue crack, together with the corresponding EBSD orientation map of the region surrounding this crack.

2.3.1 Σ3 content

The specimens have a relatively high fraction of twin boundaries, or boundaries for which the calculated misorientation relationship is 60◦ about a common [111] direction in the crystal coordinates of misoriented grains, with Σ3 boundaries making up 40% of all boundaries by length fraction, and 75% of these identified as coherent Σ3 boundaries (or 30% of the total length fraction).

2.3.2 Boundary length

The boundary smoothing procedures results in a list of grain boundary segments, each containing the grain ID number of the left- and right-hand grains which make up that segment. Segments having the same left- and right-hand grain IDs were summed together to give boundary lengths throughout the microstructure. The distribution of boundary lengths, specifically of coherent Σ3 boundaries, for the combined surface orientation maps, is plotted in Figure 2.4, with microcrack boundaries denoted by vertical lines. Note that the microcrack boundaries lie near the upper tail of the distribution.

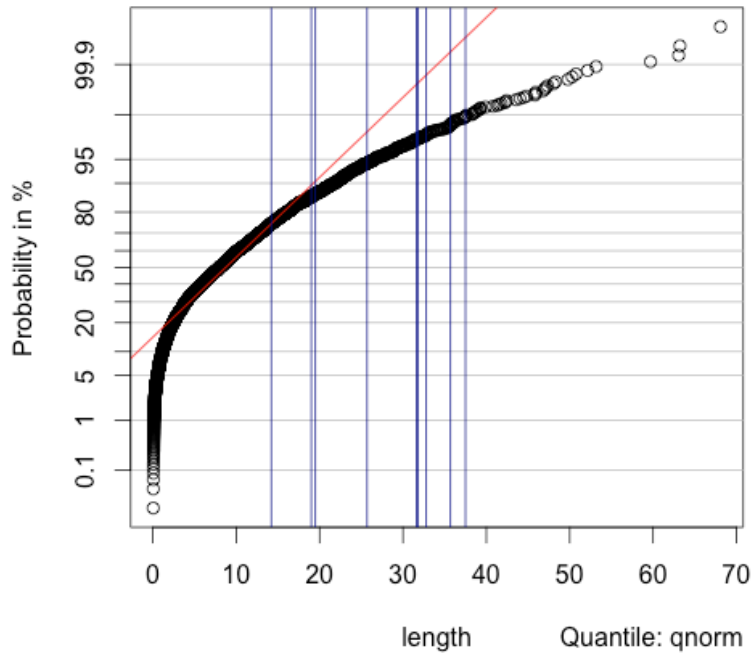

Figure 2.4. Cumulative probability plot of coherent Σ3 boundary length distribution, with microcrack boundaries indicated by vertical lines.

2.3.3 Resolved shear stress analysis

As described above, the Schmid factor is a purely geometric factor relating grain orientation to the loading direction or sample orientation, as a sort of first-order quantification of the likelihood for crystallographic slip. In a polycrystalline material, each grain is influenced by its neighbors such that the stress state cannot be assumed to be constant throughout the material. Other researchers often refer to the potential influence grain neighbors to explain material response to

cyclic loading. Given the relatively large fraction of boundaries which satisfy the first criterion for microcrack initiation, i.e. a coherent Σ3 misorientation relationship, and the low incidence of actual microcrack initiation, the phenomenon must be strongly influenced by other microstructural features. Microcrack initiation sites have clearly undergone localized plastic deformation in response to some sort of local stress concentration. In order to quantify this interaction, we consider the actual stress state in these grains by simulating the full-field anisotropic elastic stress response. In addition to the geometric Schmid factor, the simulation allows for a calculation of resolved shear stress distributions throughout the orientation map. We calculate the shear stress as resolved along coherent Σ3 boundaries, for slip systems in slip planes parallel to the boundary, for each of the crack boundary-neighboring grains.

The stress field components were then averaged to give a single set of values for each grain. These grain averaged stress field components are then combined with the smoothed and segmented boundary segment information to calculate RSS values. The RSS calculation is $RSS = \hat{b} \cdot \sigma \cdot \hat{n}$, where b is the slip direction, σ is the stress tensor, and n is the slip plane normal. Figure 2.5 is a cumulative probability plot of maximum RSS values in Σ3 boundary-adjacent grains. The RSS values were calculated using the grain-averaged stress matrix values resolved onto the three slip systems within the (111) crystallographic plane coherent with each Σ3 boundary. For each such boundary in the micrograph, a maximum RSS value was selected from the set of three values from each of the grains forming the boundary. Of note in this figure is the large number of grains with a higher probability of simulated RSS values in excess of the microcrack neighbors. Although a full-field simulation of the elastic stress response does indicate relatively high RSS values for crack-adjacent grains in a few instances, there is a broad spread of RSS values even for a small sampling of cracks.

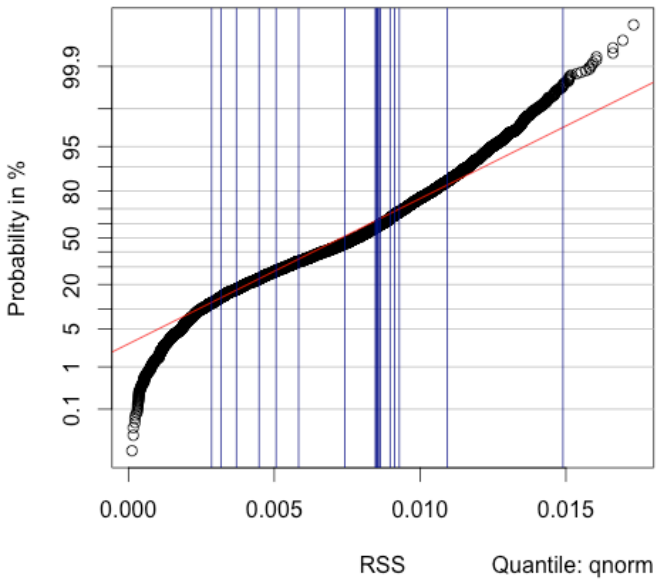

Figure 2.5. Cumulative probability distribution of maximum calculated resolved shear stress values on coherent Σ3 boundary-parallel slip planes.

Compare this distribution to that for the coherent Σ3 boundary lengths, and it is clear that there is a narrower spread of length values, with microcrack boundaries falling closer to the upper tail of the distribution.

3. Fast Fourier Transform (Spectral) Simulations

3.1 Introduction

Robust characterization techniques as used in LSHR reconstruction (see Chapter 2) provide extensive information about microstructures, presented through immense datasets. Along with most of the materials properties, mechanical responses can also be simulated via various methods. However, increase in data size leads to higher computational times, especially for standard crystal plasticity FEM simulations as complex meshing and large number of degrees of freedom are required by such calculations. Fast Fourier Transform (FFT) method developed by Moulinec and Suquet (1998) computes the effective stress-strain responses and crystallographic texture of deformed microstructures of polycrystalline materials, by using the microstructural image with orientation information as direct input. This eliminates the necessity of meshing, and decreases computational time as FFT converges on the order of Nlog[N] (Parakash and Lebensohn, 2009). FFT algorithm, later adapted for viscoplastic and small strain elasto-viscoplastic polycrystals by Lebensohn (2001, 2012), is now capable of calculating elastic and plastic responses by satisfying equilibrium and compatibility equations iteratively. It takes heterogeneity into account, but requirement of periodic boundary conditions is a limiting feature that can be handled by adding buffer layers around the sample (Lebensohn, 2012). In literature there are studies about the global convergence of FFT iteration error and effective mechanical responses, yet a sensitivity study about local field dependence on domain size was not reported. The next two parts of the report will feature the elastic FFT (elFFT) formulation and the domain size sensitivity analysis performed on LSHR specimen using elFFT.

3.2 Sensitivity Study

In the formulation of elFFT by Moulinec and Suquet (1998) for elastically heterogeneous materials, a reference medium is prepared by defining an initial homogenous reference stiffness tensor C, and an initial total strain state ε, in a way to satisfy Hooke's law

$$\sigma_{ij} = C_{ijkl}\, \varepsilon_{kl}. \tag{3.1}$$

The local fluctuations in stress, $\tau(x)$ is calculated iteratively using this reference medium and the equilibrium condition, thus resulting in

$$C^{\circ}_{ijkl}\, u_{k,lj}(x) + \tau_{ij,j}(x) = 0 \tag{3.2}$$

u_k is the displacement vector, that can be replaced using Green's function method. The symmetrized convolution integral of $\tau(x)$ and the periodic Green's function $G(x-x')$ produces the local fluctuations in strain, $\tilde{\tilde{\varepsilon}}(x)$ as

$$\tilde{\tilde{\varepsilon}}_{ij}(x) = \mathrm{sym}\left(\int G_{ik,jl}(x - x')\tau_{ij,j}(x')dx'\right). \tag{3.3}$$

Since this convolution integral can be computed in frequency space as simple multiplications,

Green's function, stress and strain fluctuations are transferred into Fourier space, and upon convergence local stress σ(x) and strain ε(x) values are calculated (Moulinec and Suquet, 1998, Lebensohn, 2012, Ghosh, 2011). A discretized grid must be created to apply FFT. This grid is directly overlaid on a 2D or 3D image. The transformation from real space into Fourier space can either be done by the implementation of numerical recipes, allowing simulation over 2^n grid points, or by using existing FFT libraries which can handle odd numbered domain sizes. For the sensitivity analysis, the elFFT code using FFTW libraries is chosen.

The near field HEDM reconstruction of the LSHR sample with surface MSFCs is used as direct input for this study. Total of 61 layers were scanned using a beam height of 4 μm in z direction and grid spacing of 0.923 μm in x and y directions. Figure 3.1 shows the full scanned volume.

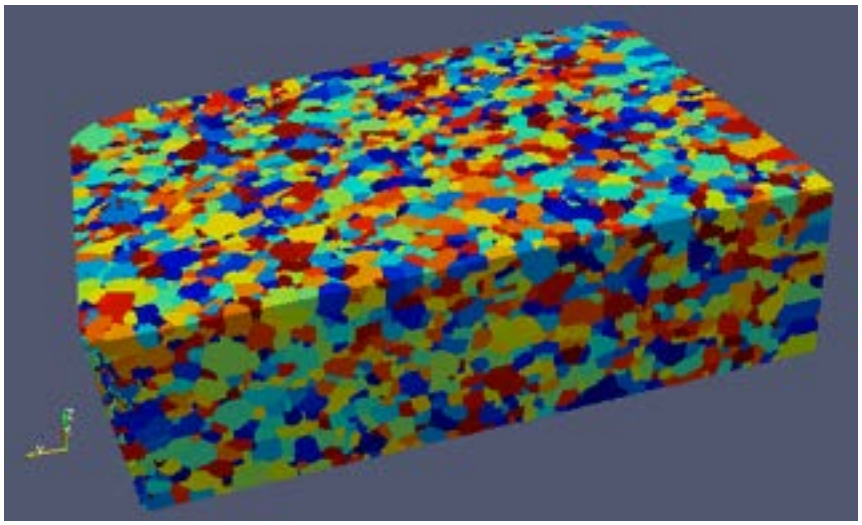

Figure 3.1. Full reconstructed volume of LSHR, with approximate dimensions 600×800×240μm.

The question is "How many neighbor grains are required for stress-strain fields to converge in a chosen grain?" In effect, this is a variant of the question "how large of a RVE is required in order to study the behavior of a specific location, in this case the region around the microcrack, in a polycrystal?" Positioning an identified crack in the center, six RVEs are trimmed out of the full volume, and the biggest one with the domain size of 512*512*64 is used as reference in the comparisons. Since the resolution of HEDM is lower at the surfaces, an optimized cut plane is applied to discard bad surface voxels. Figure 3.2 shows the structures used in simulations.

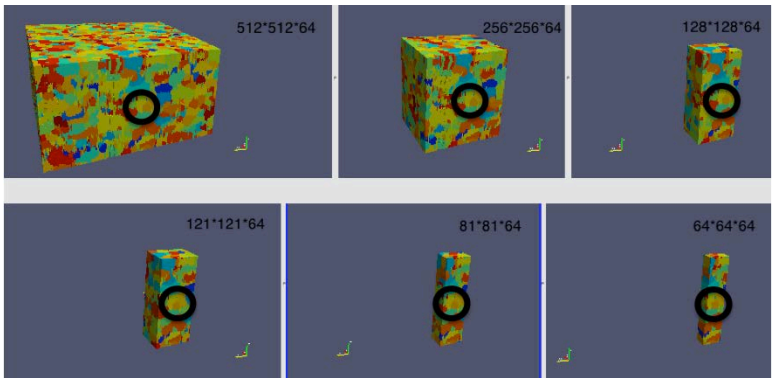

Figure 3.2. RVEs with domain sizes of 512*512*64, 256*256*64, 128*128*64, 121*121*64,

81*81*64 and 64*64*64. Identified cracked region is circled for each case.

For each RVE, identical strain boundary conditions and elastic coefficients are used to simulate elastic tension. Figure 3.3 shows the visual comparison of the maximum principal stress distributions for the grains around the microcrack.

Visual comparison suggests convergence in stress fields, which is confirmed by quantitative analysis. In table 3.1, Pearson correlation coefficients are presented for the voxel by voxel maximum principal stress comparison between reference and smaller RVEs.

Quantiative voxel by voxel comparison indicates that for a correlation bigger than 99%, 356 or more grains should exist in the simulation domain. For the LSHR specimen, the convergence trend is observed for 81*81*64 and bigger grids, as depicted in the correlation plots (Figure 3.4). This result of the sensitivity analysis remarks that at least for the elastic FFT calculation, stress-strain distributions are not very sensitive to the shape of the domain. It is not mandatory to use the entire sample in the simulations, and computation time can be decreased tremendously by trimming smaller volumes which host the region of interest.

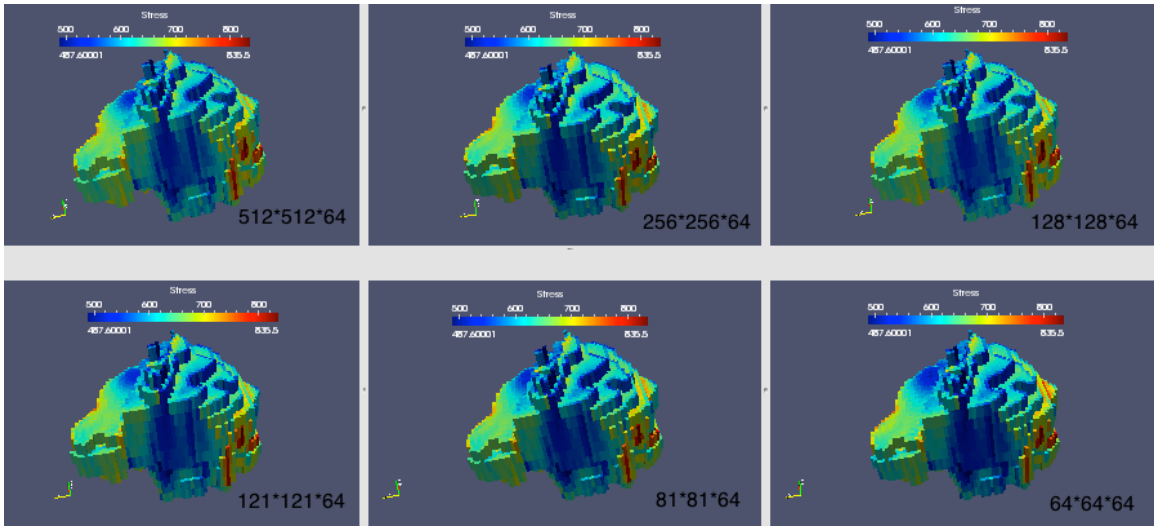

Figure 3.3. Max principal stress distributions for two neighbor grains around the identified microcrack. Stress values are rescaled with respect to the biggest RVE for comparison.

Table 3.1. Pearson Correlation Coefficients for max principal stress values within lower neighbor.

	512 vs. 256	**512 vs. 128**	**512 vs. 121**	**512 vs. 81**	**512 vs. 64**
Lower Grain (Spin: 118584)	0.9995	0.9988	0.9981	0.9944	0.9666

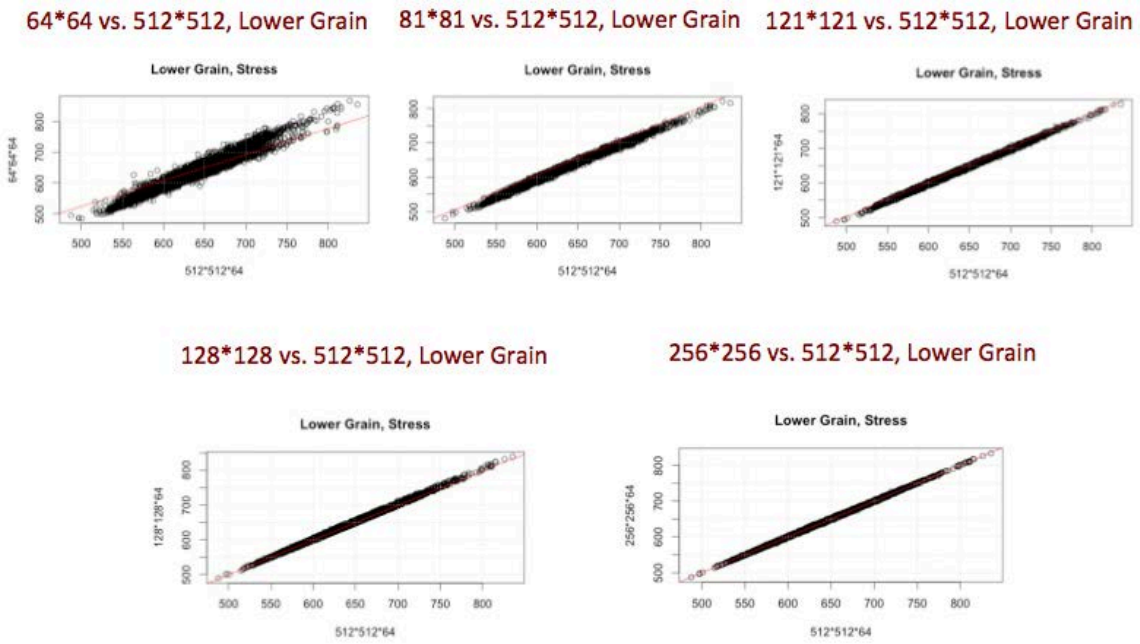

Figure 3.4. Correlation plots between the biggest RVE and others, for lower grain max principal stress values.

4. Finite Element Simulations

4.1 Introduction

Annealing twins are often referred to as strengtheners in the microstructure as their high-angle, low-energy boundaries tend to prevent the transmission of dislocations (Lim, 1984). Heavily twinned microstructures do not necessarily exhibit the classic Hall-Petch strengthening relation, and work has been done to quantify the twins' influence on the grain-size effect. Konopka and Wyrzykowski (1997) developed a relation for yield stress based on the frequency of twin boundaries that strongly or weakly oppose dislocation movement and those that act as dislocation sources. Pande *et al.* (2004) modified the Hall-Petch relation by assuming all twin boundaries act as barriers to dislocation motion (in slight opposition to Li's (1963) grain boundary strengthening arguments in which boundaries are assumed to emit dislocations) and incorporating an effective grain size term accounting for the presence of twin boundaries. Regardless of whether dislocations are prevented from transmitting across twin boundaries or are emitted from them, there is no question that dislocation pileup at twin boundaries poses severe consequences for the material's ability to resist microcrack nucleation.

It has been established that microcracks tend to nucleate at the twin boundaries of certain FCC materials such as nickel alloys (Miao *et al*., 2009; Stein *et al*., 2012) and copper (Boettner *et al*. 1964; Thompson *et al*. 1956). Why are twin boundaries favorable sites for fatigue crack formation? Heinz and Neumann (Heinz and Neumann, 1990) argued that elastic anisotropy and coherency are decisive. First, high stress concentrations develop at the twin boundaries due to elastic anisotropy. These high stresses, in turn, which can be estimated using the closed-form solution of Neumann (1999), facilitate glide at the boundaries. It is noteworthy that these high incompatibility stresses do not produce additional shear stress on the boundary plane. Rather, a

logarithmic stress singularity develops where the free surface and twin boundary trace meet. Second, alignment of the twin boundary and a slip plane (as with a coherent twin boundary) allows for dislocations to travel relatively far distances unhindered, rendering high strains under such high incompatibility stresses. Several studies have been conducted which support these claims. Miao *et al.* (2009), for example, observing the nickel-based superalloy René88DT (Krueger *et al.*, 1990) under high cycle fatigue loading, found that microcracks tended to initiate close to coherent twin boundaries in large, high-Schmid factor (soft) grains. Stein *et al.* (2012), investigating the nickel-based superalloy LSHR (Gabb *et al.*, 2005), also found that microcracks nucleated at coherent Σ3 boundaries with larger than average chord lengths at the surface.

To account numerically for these physical mechanisms, a methodology is proposed wherein high fidelity finite element models are generated from 3D high-energy X-ray diffraction microscopy (HEDM) reconstructions and coupled with a grain-size sensitive crystal plasticity model. The first part of this chapter will detail the formulation of the crystal plasticity model and explore its viability in accommodating relatively high amounts of slip on twin-parallel systems. The second part will detail the LSHR characterization effort, the steps necessary to produce a three-dimensional finite element model from a 3D HEDM dataset, and preliminary simulation efforts.

4.2 Crystal Plasticity Modeling Considerations

4.2.1 Crystal Plasticity Model Formulation

The elasto-viscoplastic crystal plasticity model follows the formulation given by Matouš and Maniatty (2004). It is implemented for FCC with twelve octahedral, {1 1 1}, and six cubic, {1 1 0}, slip systems. The resolved shear stress τ on slip system α is given by:

$$\tau^{\alpha} = \mathbf{s}^{\alpha}[\mathbf{C}^{e}\mathbf{S}]\mathbf{m}^{\alpha} \quad , \tag{4.1}$$

where **m** is the slip plane normal, **s** the slip direction, $\mathbf{C}^{e}$ the Cauchy Green Tensor, and **S** the 2nd Piola-Kirchoff Stress. The slip rate along the slip systems is given by

$$\dot{\gamma^{\alpha}} = \dot{\gamma_o} \frac{\tau^{\alpha}}{g^{\alpha}} \left| \frac{\tau^{\alpha}}{g^{\alpha}} \right|^{\frac{1}{m}-1} \quad , \tag{4.2}$$

where $\dot{\gamma^{\alpha}}$ and $\dot{\gamma_o}$ are the shear and reference shear rates, respectively, m is a material rate sensitivity parameter, and g the hardness. Hardness evolves according to a grain-size sensitivity term given by Beaudoin *et al.* (2000) and a Voce-Kocks (Kocks 1976; Voce 1955) relation, the first and second terms in Equation 4.3, respectively.

$$\dot{g^{\alpha}} = H_o \frac{\beta^2 \mu^2 b}{2(g^{\alpha} - g_o^{\alpha})} \sum_{\kappa=1}^{N_{ss}} \sqrt{\Delta_{iJ} m_j \Delta_{kL} m_L} \left| \dot{\gamma^{\kappa}} \right| + G_o \left(\frac{g_s^{\alpha} - g^{\alpha}}{g_s^{\alpha} - g_o^{\alpha}} \right) \sum_{\kappa=1}^{N_{ss}} \left| \dot{\gamma^{\kappa}} \right| \quad , \tag{4.3}$$

H_o and G_o in Equation 4.3 are rate coefficients, β = 1/3, b is the Burgers vector, and g_o and g_s are initial and saturation resolved shear strengths, respectively. The Δ variable in the first term

of the hardness evolution is a dislocation density term, a measure of lattice incompatibility, and is expressed as a function of the plastic deformation:

$$\Delta_{iJ} = \boldsymbol{\epsilon}_{JKL}\mathbf{F}^{p}_{iL,K} \tag{4.4}$$

This measure is appropriate for modeling annealing twins because high gradients of plastic deformation develop across their boundaries. Consequently, geometrically-necessary dislocations localize close to the boundaries to accommodate these high gradients (Ashby 1970). The Δ term effectively accounts for this phenomenon by considering the gradient of the plastic deformation gradient, accommodating the evolution of slip close to twin boundaries. It is noteworthy that the Voce-Kocks relation in Equation 4.3 is a slight departure from that given in the original formulation of the crystal plasticity model (Matouš and Maniatty, 2004). Here, latent and self-hardening effects are not assumed equal; consequently, the slip systems do not harden at the same rate. This is to allow the preference for slip on the twin-parallel systems discussed earlier.

Optionally, to supplement the implicit hardening effects of the model, the critical resolved shear stress values assigned to twin-parallel systems are scaled to be lower than those of non-twin-parallel systems. The idea here is that for systems with relatively long slip line lengths (as with twin-parallel systems), the lower critical resolved shear stress facilitates the evolution of slip on those systems, thereby replicating physically observed phenomena. To accomplish this, the four {111} slip planes are centered at the grain's centroid. For each slip plane, the shortest distance between the centroid and trace of grain surface on the slip plane is recorded. The scaling, finally, is accomplished by considering the ratio of the longest slip line length to the shortest. Twin lamellae exhibit the highest ratios (~6) while equi-axed grains show no preference, meaning that this scaling only effects grains with elongated morphologies.

4.3 Exploratory Simulations

4.3.1 The Baseline Model

A relatively simple, idealized finite element model of a twin lamella and its containing grain was generated for the purposes of probing the sensitivity of slip localization to orientation, twin lamella length, and twin-containing grain size, offering a means to gauge the effectiveness of the crystal plasticity model at accommodating slip on twin-parallel systems. The twin and its containing grain, surrounded by a cubical as-large-as (ALA) grain for load-transfer purposes, could be assigned orientations to yield coherent twin boundaries, Figure 4.1.

A baseline model with coherent twin boundaries is considered here. Figure 4.2(a) shows accumulated slip on the twin lamella without the scaling discussed earlier. It is apparent that slip evolved from the lamella's edges inward. Moreover, approximately 80% of total slip on the twelve octahedral slip systems was on the twin-parallel systems. A baseline model without the twin lamella is considered next to gauge the crystal plasticity model's ability to accommodate slip on twin-parallel systems without long, slender twin morphologies. Here, the twin lamella, labeled B in Figure 4.1, was merged into half of the twin-containing grain, region C, leaving a coherent $\Sigma 3$ boundary between grains BC and A. Figure 4.2(b) and Figure 4.2(c) show the evolution of slip in grain A without and with scaling of the twin parallel systems, respectively.

Without scaling, approximately 75% of total slip on the octahedral slip systems was on the boundary-parallel systems. With scaling, this percentage rose to 80%. For all three of these simulations, it is noteworthy that the highest localizations of slip occurred at the coherent boundaries. One could extend this observation to the idea of hotspots and the identification of potential microcrack nucleation sites (Rollett *et al*., 2010).

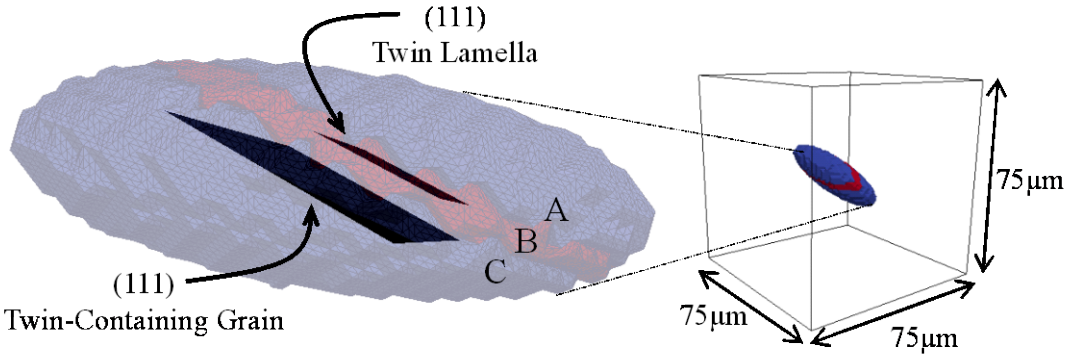

Figure 4.1. The baseline model showing alignment of the (111) slip planes of the twin lamella and twin-containing grain with the twin boundaries, rendering coherent twin boundaries.

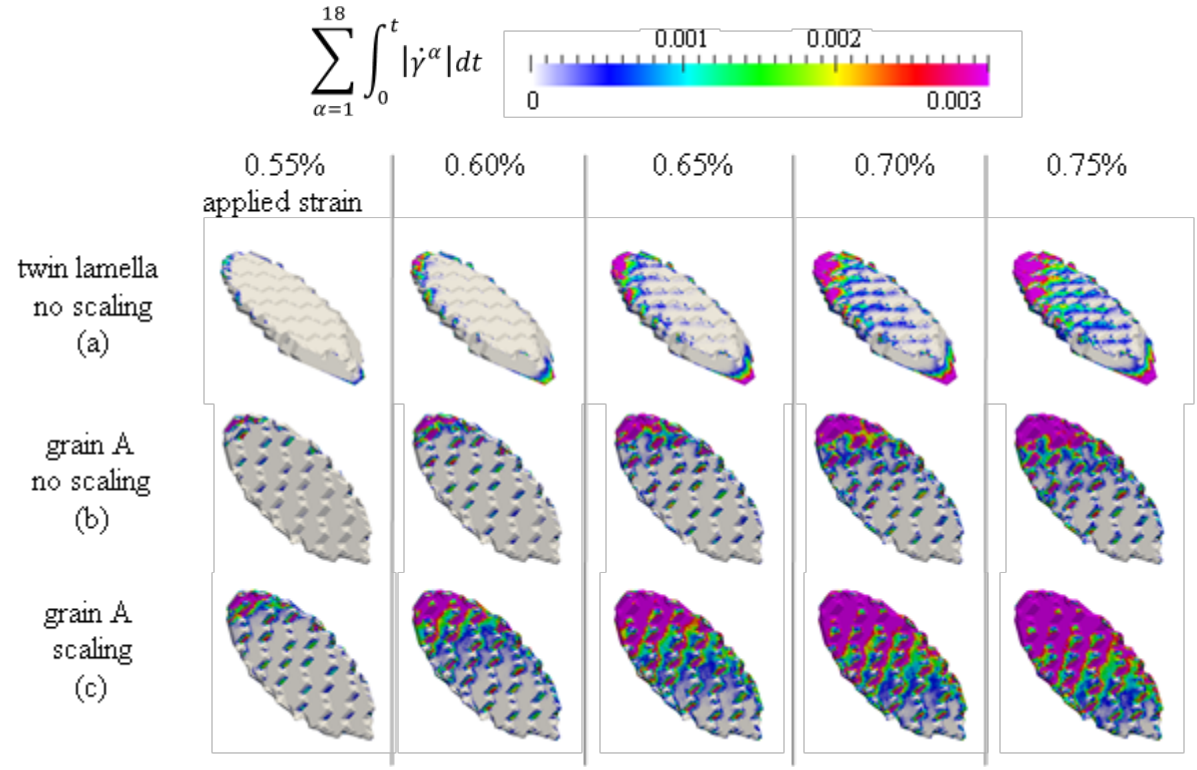

Figure 4.2. Evolution of slip in baseline model on twin lamella without scaling (a), grain A without twin lamella and no scaling (b), and grain A without twin lamella and with scaling (c).

Next, the evolution of slip around coherent and incoherent Σ3 boundaries in the baseline model is considered. Here, once-coherent slip systems were incrementally rotated out-of-phase with the boundary to gauge the influence coherency has on the extent of the resulting hotspot, Figure 4.3. From the simulations, it is apparent that as once-coherent planes became increasingly misaligned

with the boundary, the extent of the hotspot lessened. Consequently, it seems that coherency plays a decisive role in slip localization close to a Σ3 boundary.

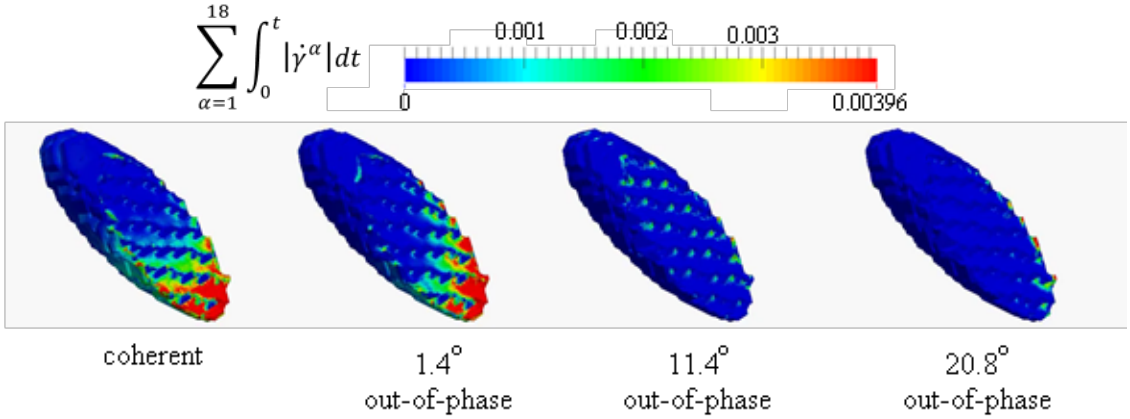

Figure 4.3. Evolution of slip in Grain A of baseline model for coherent and incoherent Σ3 boundaries at 0.60% applied strain.

4.3.2 Heavily Twinned, Synthetic Polycrystal

A statistically representative, synthetic polycrystal of the nickel-based superalloy René88DT was generated for the purposes of probing the crystal plasticity model's ability to accommodate relatively high amounts of slip along annealing twin boundaries. The polycrystal, Figure 4.4(a), contained thirty twin-parent grain instances, and all twin boundaries were coherent Σ3 boundaries. It was loaded in simple tension to 0.75% strain. For the purposes of this study, a hotspot was deemed a significant localization of slip (both in extent and magnitude), Figure 4.4(b). 27 of these localizations were identified, and of these 27, 17 (63%) participated in twin-parent morphologies. This result suggests that gradient plasticity allows for the preference for slip to accumulate along twin boundaries.

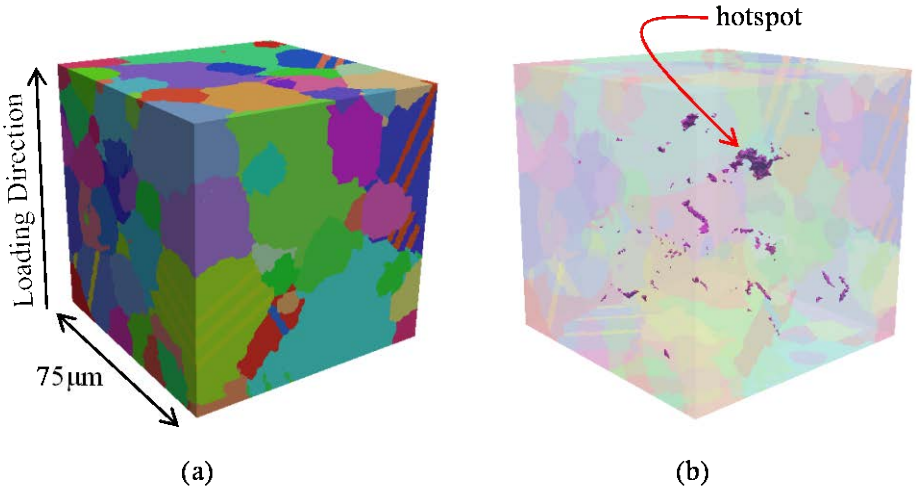

Figure 4.4. Synthetic polycrystal of René88DT with annealing twins (a) and hotspots in synthetic volume at 0.75% applied strain (b).

4.3.3 LSHR Reconstruction

The reconstructed LSHR volume (see Chapter 2) was imported into the microstructure analysis and generation software DREAM.3D (Jackson and Groeber, 2013) as a .ph file. The resolution was specified to yield an 82.0 x 235.5 x 256.0 μm volume, Figure 4.5. A multiple-material marching cubes (M3C) (Wu and Sullivan, 2003) algorithm was specified in DREAM.3D to mesh each generated grain. This procedure was preferred over the traditional marching-cubes algorithm as it rendered a surface mesh of the entire volume with conformal grain boundaries without voids or penetrations. The surface mesh of each grain was output in binary stereolithography (STL) files.

A volumetric meshing algorithm given by Cavalcante *et al*. (2001 and 2005) was then exposed for the purposes of discretizing the volume of each grain with tetrahedra. The resulting 1,229-grain mesh was composed of 10,700,578 quadratic tetrahedra. This 45-million degree-of-freedom (DOF) model necessitated the exploitation of a massively parallel finite element driver for use in a high performance computing environment. One such driver used in this investigation was Finite Element All-Wheel Drive (FEAWD), a MPI-based code built on FemLib (a library of constitutive models and finite elements), Boost, the BLAS and LAPACK, PETSc, ParMETIS, and HDF5. Stampede, Texas Advanced Computing Center's Dell Linux cluster, was the primary computational resource used for the simulations discussed in this chapter.

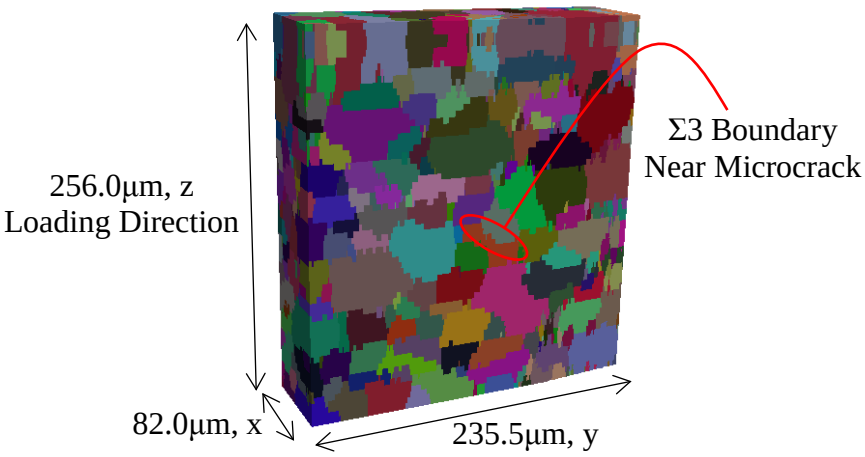

Figure 4.5. Reconstructed 1,229-grain volume containing the microcrack close to the Σ3 boundary discussed in Chapter 2.

The model was loaded monotonically in simple tension. The grains were assigned orientations from the aforementioned forward modeling reconstruction procedure. Slip began to localize on the free surface at approximately 0.45% applied strain; however, these localizations were not near the coherent Σ3 boundary in question. For increasing load, slip eventually did accumulate near this boundary, but this was after more significant localizations developed elsewhere on the free surface, Figure 4.6. Work with this reconstruction is still ongoing.

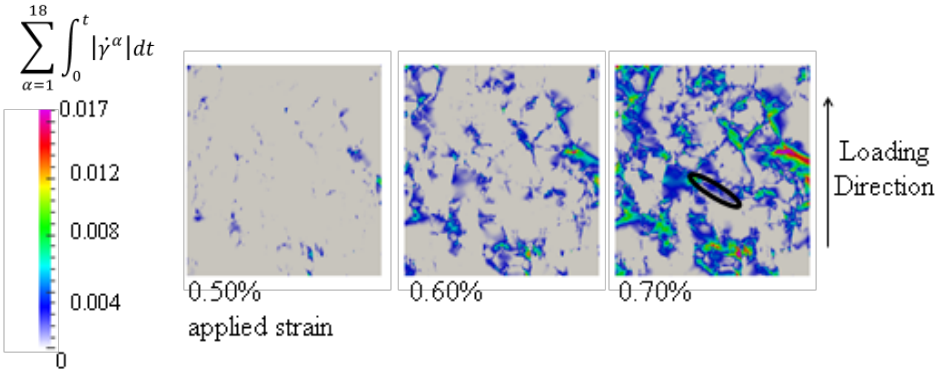

Figure 4.6. Evolution of slip in reconstruction model. The Σ3 boundary discussed in Chapter 2 is circled in black.

5. Summary

- Investigation of cracks of the order of the grain size showed very clearly that crack initiation is strongly correlated with accumulated slip parallel to twin boundaries in large grains with high Schmid factors.
- High Energy Diffraction Microscopy (HEDM) was successfully performed on both micro-cracked LSHR and on two halves of a fully fractured fatigue sample of Rene 88DT.
- The LSHR HEDM dataset was used to instantiate simulation volumes of various sizes.
- Simulation of 3D microstructures representing the well-aligned grains against twin boundaries showed the same hot spots in accumulated slip as seen in experiment.
- Use of a constitutive relationship that includes the effect of gradients in plastic deformation was key to modeling the hot spots in crystallographic slip.

6. Publications:

Stein, C., Lee, S., and Rollett, A. (2012). "An Analysis of Fatigue Crack Initiation Using 2D Orientation Mapping and Full-Field Simulation of Elastic Stress Response." *Superalloys 2012*, Champion, PA.

Cerrone, A., Spear, A., Tucker, J., Stein, C., Rollett, A., and Ingraffea, A. (2013). "Modeling Crack Nucleation At Coherent Twin Boundaries In Nickel-based Superalloys." *MS&T'13*, Montréal, Quebec, Canada.

Tucker, J., Cerrone, A., and Rollett, A. (2013). "An analysis of full-field three-dimensional elasto-viscoplastic finite element simulations of René88DT microstructure for low cycle fatigue." In preparation.

Related Publications:

Donegan, S. P., Tucker, J. C., Rollett, A. D., Barmak, K., and Groeber, M. (2013). "Extreme Value Analysis of Tail Departure from Log-Normality in Experimental and Simulated Grain Size Distributions." *Acta Materialia*. In Press.

Semiatin, S. L., McClary, K. E., Rollett, A. D., Roberts, C. G., Payton, E. J., Zhang, F., and Gabb, T. P. (2012). "Microstructure Evolution during Supersolvus Heat Treatment of a Powder Metallurgy Nickel-Base Superalloy." *Metallurgical and Materials Transactions A*, 43(5), 1649–1661.

Tucker, J. C., Chan, L. H., Rohrer, G. S., Groeber, M. A. and Rollett, A. D. (2011) “Tail Departure of Log-Normal Grain Size Distributions in Synthetic Three-Dimensional Microstructures.” *Metallurgical and Materials Transactions A*. 43(8):2810–2822.

Tucker, J. C., Chan, L. H., Rohrer, G. S., Groeber, M. A., and Rollett, A. D. (2012). “Comparison of grain size distributions in a Ni-based superalloy in three and two dimensions using the Saltykov method.” *Scripta Materialia*, Acta Materialia Inc., 66(8), 554–557.

Y. S. Choi, Groeber, M. A., Shade, P. A., Turner, T. J., Schuren, J. C., Dimiduk, D. M., Uchic, M. D., Woodward, C., Rollett, A. D., and Parthasarathy, T. A. (2013). “Crystal Plasticity Finite Element Method Simulations for a Polycrystalline Ni Micro-Specimen Deformed in Tension.”

7. People

A.D. Rollett was the PI on the project, with Tony Ingraffea as co-PI at Cornell. Clayton Stein, PhD student, was responsible for microstructural characterization of the materials examined in the project. Joseph Tucker, PhD student, worked on the related topic of reconstruction of 3D microstructures in the computer. Tucker was supported by other projects, including General Electric in part. Tugce Ozturk, PhD student, worked on the sensitivity analysis of elastic Fast Fourier Transform simulation. Albert Cerrone at Cornell University worked on finite element simulation of elastoplastic deformation. Several individuals in the group of Prof. Robert Suter (Physics, CMU) assisted with HEDM data acquisition, especially Jonathan Lind, Frankie Li and Reeju Pokharel.

8. References

Ashby, M. F. (1970). “The deformation of plastically non-homogeneous materials.” *Philosophical Magazine*, 21(170), 399–424.

Beaudoin, A. J., Acharya, A., Chen, S. R., Korzekwa, D. A., and Stout, M. G. (2000). “Consideration of grain-size effect and kinetics in the plastic deformation of metal polycrystals.” *Acta Materialia*, 48(13), 3409–3423.

Boettner, R. C., McEvily, A. J., and Liu, Y. C. (1964). “On the formation of fatigue cracks at twin boundaries.” *Philosophical Magazine*, 10(103), 95–106.

Cavalcante Neto, J. B., Wawrzynek, P. A., Carvalho, M. T. M., Martha, L. F., and Ingraffea, A. R. (2001). “An Algorithm for Three-Dimensional Mesh Generation for Arbitrary Regions with Cracks.” *Engineering With Computers*, 17(1), 75–91.

Cavalcante-Neto, J. B., Martha, L. F., Wawrzynek, P. A., and Ingraffea, A. R. (2005). “A back-tracking procedure for optimization of simplex meshes.” *Communications in Numerical Methods in Engineering*, 21(12), 711–722.

El Bartalia, A., Aubina, V., Sabatiera, L., Villechaiseb, P., and Degallaix-Moreuila, S. (2008). “Identification and analysis of slip systems activated during low-cycle fatigue in a duplex stainless steel.” *Scripta Materialia*, 59(12), 1231–1234.

Gabb, T., Gayda, J., Telesman, J., and Kantzos, P. (2005). “Thermal and mechanical property characterization of the advanced disk alloy LSHR.” (June).

Ghosh, S., Dimiduk, D. (2011). "Computational Methods for Microstructure-Property Relationships." (New York: Springer).

Heinz, A., and Neumann, P. (1990). “Crack initiation during high cycle fatigue of an austenitic steel.” *Acta Metallurgica et Materialia*, 38(10), 1933–1940.

Jackson, M., and Groeber, M. (2013). “DREAM.3D.” BlueQuartz Software.

Kocks, U. F. (1976). “Laws for work-hardening and low-temperature creep.” *ASME, Transactions, Series H-Journal of Engineering Materials and Technology*, 98, 76–85.

Konopka, K., and Wyrzykowski, J. W. (1997). “The effect of the twin boundaries on the yield stress of a material.” *Journal of Materials Processing Technology*, 64(1-3), 223–230.

Krueger, D., and Kissinger, R. (1990). "Fatigue crack growth resistant nickel-base article and alloy and method for making." U.S. Patent #4957567.

Lebensohn, R. A. (2001). “N-site modeling of a 3D viscoplastic polycrystal using Fast Fourier Transform.” *Acta Materialia*, 49(14), 2723–2737.

Lebensohn, R. A. *et al*. (2012). “An elasto-viscoplastic formulation based on fast Fourier transforms for the prediction of micromechanical fields in polycrystalline materials.” *International Journal of Plasticity*, (32):59–69.

Li, J. C. M. (1963). “Petch relation and grain boundary sources.” *Trans. TMS-AIME*, 277, 239–247.

Lienert, U., Almer, J., Jakobsen, B., Pantleon, W., Poulsen, H. F., Hennessy, D., Xiao, C., and Suter, R. M. (2007). “3-Dimensional Characterization of Polycrystalline Bulk Materials Using High-Energy Synchrotron Radiation.” *Materials Science Forum*, 539-543, 2353–2358.

Lim, L. C. (1984). “Slip-twin interactions in nickel at 573K at large strains.” *Scripta Metallurgica*, 18(10), 1139–1142.

Lorensen, W. E., Cline, H. E. (1987). "Marching cubes: A high resolution 3D surface construction algorithm," *ACM*, vol 21.

Marinelli, M.-C., El Bartali, A., Signorelli, J. W., Evrard, P., Aubin, V., Alvarez-Armas, I., and Degallaix-Moreuil, S. (2009). “Activated slip systems and microcrack path in LCF of a duplex stainless steel.” *Materials Science and Engineering: A*, 509(1-2), 81–88.

Matouš, K., and Maniatty, A. M. (2004). “Finite element formulation for modelling large deformations in elasto-viscoplastic polycrystals.” *International Journal for Numerical Methods in Engineering*, 60(14), 2313–2333.

Miao, J., Pollock, T. M., and Wayne Jones, J. (2009). “Crystallographic fatigue crack initiation in nickel-based superalloy René 88DT at elevated temperature.” *Acta Materialia*, Acta Materialia Inc., 57(20), 5964–5974.

Miao, J., Pollock, T. M., and Wayne Jones, J. (2012). “Microstructural extremes and the transition from fatigue crack initiation to small crack growth in a polycrystalline nickel-base superalloy.” *Acta Materialia*, Acta Materialia Inc., 60(6-7), 2840–2854.

Moulinec, H., and Suquet, P. (1998). “A numerical method for computing the overall response of nonlinear composites with complex microstructure.” *Computer Methods in Applied Mechanics and Engineering*, 157(1-2), 69–94.

Mu, P., and Aubin, V. (2010). “Microcrack initiation in low-cycle fatigue of an austenitic stainless steel.” *Procedie Engineering*, 2(1), 1951–1960.

Neumann, P., and Tonnessen, A. (1987). “Cyclic Deformation and Crack Initiation.” *Third International Conference on Fatigue and Fatigue Thresholds*, Charlottesville, VA.

Neumann, P. (1999). “Analytical Solution for the Incompatibility Stresses at Twin Boundaries in Cubic Crystals.” *Fatigue 99*, Beijing, 107–114.

Newman Jr., J. C. (2000) “Advances in Fatigue and Fracture Mechanics Analyses for Metallic Aircraft Structures.” *Proc. 20th ICAF Symposium of the Int. Committee on Aeronautical Fatigue, Bellevue, Washington, Plantema Memorial Lecture*. 3-42.

Pande, C. S., Rath, B. B., and Imam, M. A. (2004). “Effect of annealing twins on Hall–Petch relation in polycrystalline materials.” *Materials Science and Engineering: A*, 367(1-2), 171–175.

Peralta, P. and Laird, C. (1997). "Compatibility stresses in fatigued bicrystals: Dependence on misorientation and small plastic deformations." *Acta Materialia*, 45(12):5129– 5143.

Prakash, A. and Lebensohn, R. A. (2009). "Simulation of micromechanical behavior of poly-crystals: finite elements versus fast Fourier transforms." *Modelling and Simulation in Materials Science and Engineering*, 17(6):064010.

Rollett, A. D., Lebensohn, R. A., Groeber, M., Choi, Y., Li, J., and Rohrer, G. S. (2010). “Stress hot spots in viscoplastic deformation of polycrystals.” *Modelling and Simulation in Materials Science and Engineering*, 18(7), 074005.

Stein, C., Lee, S., and Rollett, A. (2012). “An Analysis of Fatigue Crack Initiation Using 2D Orientation Mapping and Full-Field Simulation of Elastic Stress Response.” *Superalloys 2012*, Champion, PA.

Suter, R. M., Hennessy, D., Xiao, C., and Lienert, U. (2006). “Forward modeling method for microstructure reconstruction using x-ray diffraction microscopy: Single-crystal verification.” *Review of Scientific Instruments*, 77(12), 123905.

Suter, R. M., Hefferan, C. M., Li, S. F., Hennessy, D., Xiao, C., Lienert, U., and Tieman, B. (2008) "Probing Microstructure Dynamics With X-Ray Diffraction Microscopy." *Journal of Engineering Materials and Technology*, 130(2):021007.

Thompson, N., Wadsworth, N., and Louat, N. (1956). “The origin of fatigue fracture in copper.” *Philosophical Magazine*, 1(2), 113–126.

Voce, E. (1955). “A practical strain-hardening function.” *Metallurgica*, 51(307), 219–226.

Wu, Z., and Sullivan, J. M. (2003). “Multiple material marching cubes algorithm.” *International Journal for Numerical Methods in Engineering*, 58(2), 189–207.

Related References:

Brockenbrough, J. R., Hinkle, A. J., Magnusen, P. E. and Bucci, R. J. (1994). “Microstructurally based model of fatigue initiation and growth.” DTIC Document.

Thompson, A. W. and Backofen, W. A. (1971). “The effect of grain size on fatigue.” *Acta Metallurgica*. 19(7):597–606.

Thompson, A. W. (1972). “The influence of grain and twin boundaries in fatigue cracking.” *Acta Metallurgica*. 20(9):1085–1094.

Thompson, A. W. and Bucci, R. J. (1973). “The dependence of fatigue crack growth rate on grain size.” *Metallurgical and Materials Transactions B*.

Tucker, J. C., Chan, L. H., Rohrer, G. S., Groeber, M. A. and Rollett, A. D. (2012). “Comparison of grain size distributions in a Ni-based superalloy in three and two dimensions using the Saltykov method.” *Scripta Materialia*, 66(8):554–557.